SLAC-R-1080

High Power, Magnet-free, Waveguide Based Circulator Using Angular-Momentum Biasing of a Resonant Ring

Jeffrey Neilson and Emilio Nanni

August 18, 2017

Prepared for Calabazas Creek Research, Inc. under Work for Others Agreement (WFOA) No. 16-0

SLAC National Accelerator Laboratory, 2575 Sand Hill Road, Menlo Park, CA 94025

This material is based upon work supported by the U.S. Department of Energy, Office of Science, Office of High Energy Physics, under Contract DE-AC02-76SF00515.

Summary

Existing and future high power accelerators require RF power transmission components capable of handling high average-power (CW or high duty factor) with low loss and high reliability. Typically the RF power for these accelerators is generated using high power klystrons. The klystrons operate with high electric field gradients in the output cavity, and it is these field gradients that often limit the power capability of the device. When an abnormal event occurs in the waveguide system, such as an arc, power is reflected back toward the klystron. This can cause a sudden, dramatic increase in electric field level at the output window and across the gap(s) of the output cavity, invariably leading to severe breakdown. In many cases, this results in destruction of the tube, either from breakage of the output window or damage to the output cavity drift tube tips. Since arcing is a fairly routine event, especially during initial processing of the waveguide system, it is necessary to provide some means of protecting the klystron from damage.

A common device for protecting an RF source from reflected power is the waveguide circulator. A circulator is typically a three-port device that allows low loss power transmission from the source to the load, but diverts power coming from the load (reflected power) to a third terminated port. Circulators are currently available at X-Band for power levels up to 1 MW in waveguide configurations; however, the next generation of RF sources for high gradient accelerators will require circulators in the 50-100 MW range. Conventional ferrite based circulator technology is not capable of reaching the power level required.

In this report, we have evaluated a new class of circulator which appeared to have potential for operation at power levels greatly exceeding current technology. The circulator employs a new concept to generate non-reciprocal behavior without the use of ferrite materials. The novel circulator approach is based on parametric modulation of three, identical, coupled resonators generating non-reciprocal behavior as proposed by Estep[1]. The resonant frequencies of three symmetrically coupled cavities are modulated by an external RF driver at the same amplitude and a relative phase difference of 120 degrees. This cavity modulation imparts an effective electronic angular momentum to the system and generates the non-reciprocal behavior of a circulator.

Multiple configurations for a waveguide based implementation of the ferrite free circulator concept were evaluated in this program. The best performance obtained (return loss -12.5 dB, insertion loss -1.3 dB and isolation -15.4 dB) is not good enough to warrant further development of this approach unless new techniques and lower loss material can be found that could provide adequate performance. For high power klystron applications, a typical acceptable performance level would be return and isolation < -20 dB and an insertion loss < 0.5 dB.

1 Estep, Nicholas A., et al. "Magnetic-free non-reciprocity and isolation based on parametrically modulated coupled-resonator loops." *Nature Physics* 10.12 (2014): 923-927

Theory

In a recent development, Estep[1] demonstrated that an effective "electronic spin" could be imparted on a system of three identical coupled cavities whose coupled resonant frequency is at the RF input frequency and where that resonant frequency is spatiotemporally modulated by an external modulation frequency applied to each individual cavity. The geometry for this

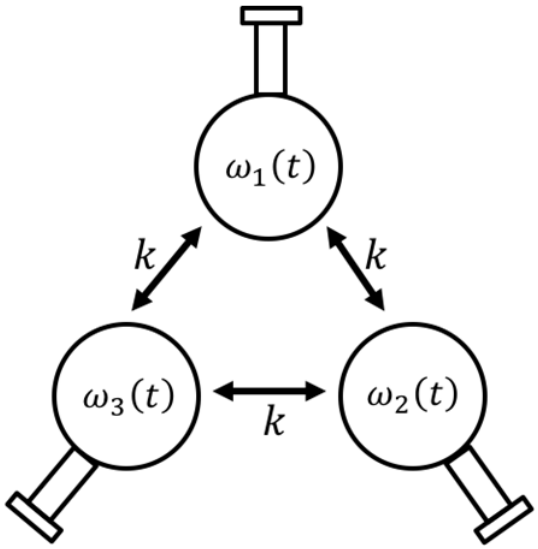

Figure *1*. Set of three symmetrically coupled cavities. The resonant frequencies of the cavities are modulated as $\omega_1(t) = \omega_o + \delta\omega_m \cos(\omega_m t), \omega_2(t) = \omega_o + \delta\omega_m \cos(\omega_m t + 2\pi/3), \omega_3(t) = \omega_o + \delta\omega_m \cos(\omega_m t + 4\pi/3)$ and are coupled together with a cavity coupling coefficient of magnitude k. The cavity coupling magnitude k and resonant frequency ω_o are adjusted so the resonate frequency of the coupled three cavity system is equal to the external RF source frequency ω_{RF}. The resonant frequency of the individual cavities is modulated at a frequency ω_m where $\omega_m \ll \omega_{RF}$.

configuration is shown in **Error! Reference source not found.**. A proper phasing of the modulating signal breaks the degeneracy of the clockwise and counter clockwise propagating waves that exist in this
configuration of coupled cavities. This results in a non-reciprocal behavior to a RF source connected to one of the cavity ports, with power being distributed unequally between the other two ports. High directivity (large difference between power split to output ports) can be achieved by adjusting the parameters controlling the non-reciprocal behavior, thereby resulting in the behavior of a three-port circulator. Using temporal coupled mode theory [1] we have modeled this behavior for the three-cavity configuration of Figure 1 with three external coupling ports:

$$\frac{da_1}{dt} = (-i\omega_1(t) - 1/\tau)a_1 - ika_2 - ika_3 + d\,S^+ \quad \text{(Eq 1)}$$

$$\frac{da_2}{dt} = (-i\omega_2(t) - 1/\tau)a_2 - ika_1 - ika_3 \quad \text{(Eq 2)}$$

$$\frac{da_3}{dt} = (-i\omega_3(t) - 1/\tau)a_3 - ika_1 - ika_2 \quad \text{(Eq 3)}$$

$$S_i^- = -S_i^+ + d\,a_i \quad \text{(Eq 4)}$$

$$d = \sqrt{2/\tau_{external}} \quad \text{(Eq 5)}$$

$$\tau = 2Q_o/\omega_{rf} + 2Q_{ext}/\omega_{rf} \quad \text{(Eq 6)}$$

where a_i is the amplitude of the ith cavity field, S_i are the incident (+) and reflected (-) amplitudes at the ith port, $\omega_m, \delta\omega_m$ are the cavity frequency modulation rate and depth respectively, and the remaining parameters are as defined in Figure 1. Equations 1-3 can be solved in a Runge-Kutta formulation for the parameters $k, Q, \omega_m, \delta\omega_m$ to yield the time varying cavity amplitudes $a_i(t)$. Computing the port amplitudes with Equation 4 and transforming to the frequency domain yields the frequency power spectrum for each port, which can be used to determine the directivity and S parameters of the device.

Several tests were done to validate our Runge-Kutta solution of the couple mode equations. In the first test, the case of no external port coupling and a delta function excitation of one cavity was tested with cavity parameters $\omega_o = 2\pi$ 3.0 GHz and $k = 2\pi$ 0.2 GHz. The frequency domain response of the cavity is shown in Figure 2. Two peaks in the frequency spectrum are seen, one at $\omega_o - k$ and the other at $\omega_o + 2k$. These are the frequencies that are predicted by analytic coupled cavity theory, with the resonance $\omega_o + 2k$ being the mode where all cavities fields at the same phase and $\omega_o - k$ is a degenerate, rotating mode with $\pm 2\pi/3$ phase shift between cavity fields.

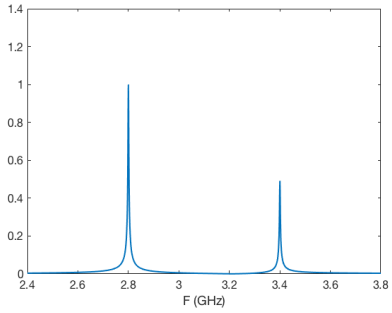

Figure 2 Frequency domain response of three coupled cavities to a transient excitation.

In the second test, three cavities with external ports (Figure 3) were modeled in HFSS (a finite element code for simulating high-frequency electromagnetic fields). The external Q of the cavities was set to 100 by adjustment of the waveguide coupling width, and cavity Q and resonant frequency ω_o were determined from calculation for a single standalone cavity. The coupling factor k is determined from the two calculated Eigen frequencies ω_1 and ω_2 of the three coupled cavities (given by one third of the frequency separation of the two modes). The values of Qo, Qext, ω_o and k were then used in the solution for equations 1-4 to obtain the reflected and transmitted power for ports 1 and 2 (S11 and S21 respectively). The results are shown in Figure 3 along with the HFSS calculations. Very good agreement between the HFSS and coupled mode theory (CMT) calculation was achieved.

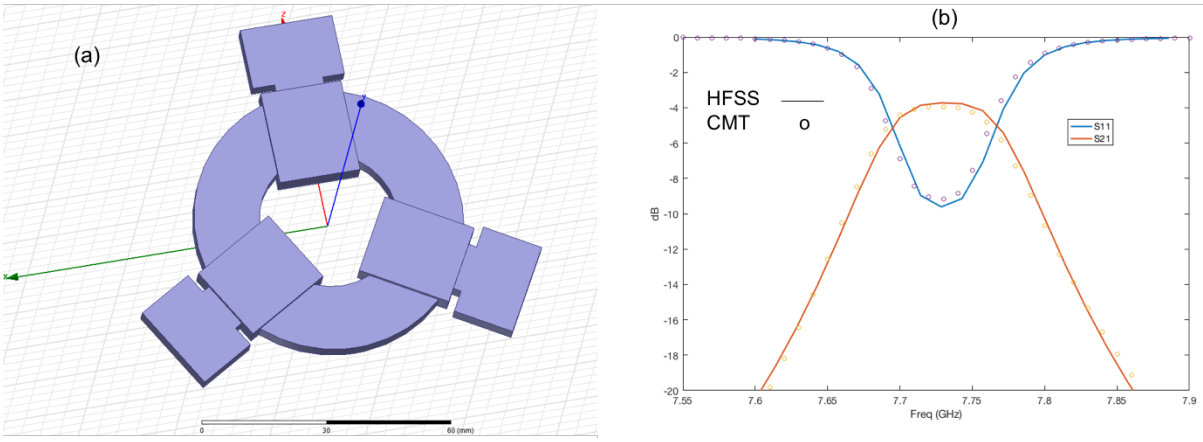

Figure 3 Calculation comparison between HFSS and CMT. (a) Cavity geometry (b) Return and transmission loss (dB)

Figure 4 shows the case with a drive signal at the rotating mode frequency on port 1 with no modulation of the cavities resonant frequency. As expected the power fed into cavity 1 is split equally between ports 2 and 3.

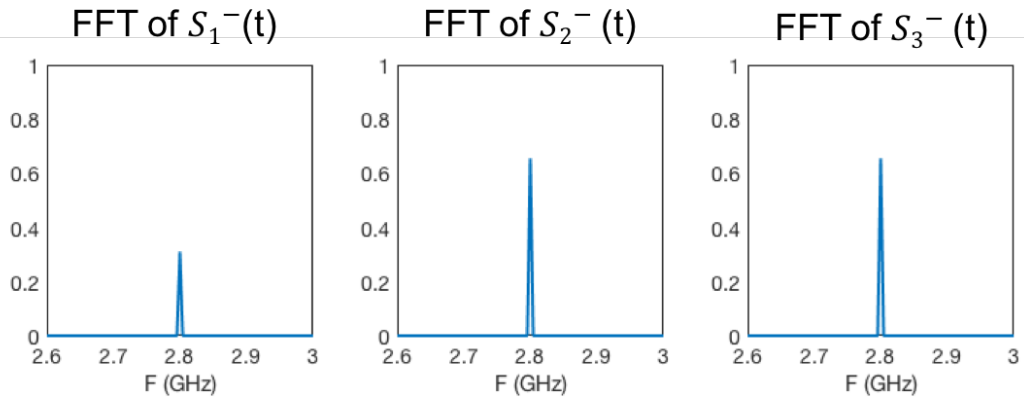

Figure 4 Frequency domain response of signal leaving three ports with constant excitation on port 1.

By proper adjustment of the modulation parameters ($\omega_m, \delta\omega_m$) and cavity coupling strength (k), one can create a condition where the non-reciprocal behavior induced by the modulation results in a coherent cancellation of the power in one of the cavities. This is shown in Figure 5 where the power fed into cavity one appears in cavity two while the amplitude in cavity three is near zero. Since the system is symmetric under rotation, power fed into cavity two will appear in cavity three and power fed into cavity three will appear in cavity one. This is the behavior of a three port circulator. To minimize coupling between the common mode and the rotating modes, the modulation rate must be much less than the frequency separation of the modes. This frequency difference is equal to three times the cavity coupling magnitude k.

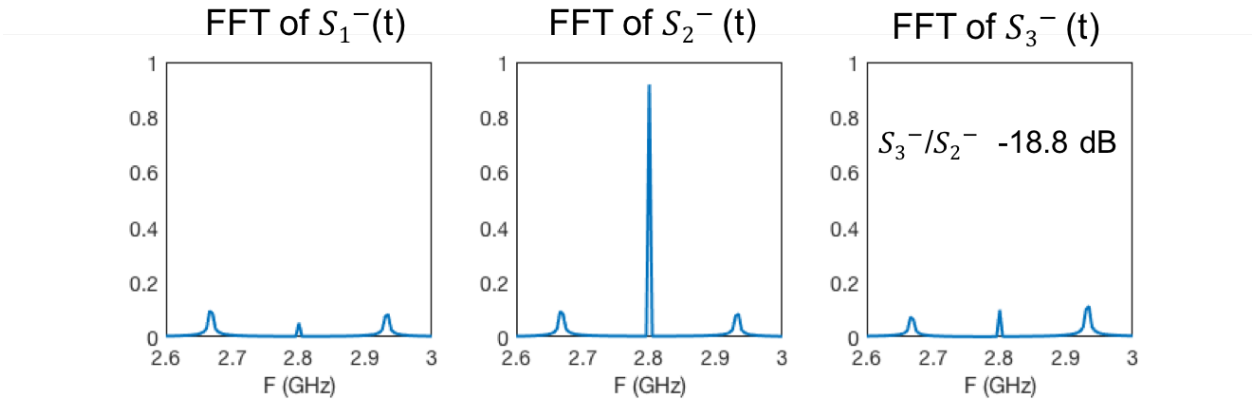

Figure 5 Frequency domain response of signal leaving three ports with constant excitation on port 1 and cavity frequency modulated as $\omega_1(t) = \omega_o + \delta\omega_m \cos(\omega_m t), \omega_2(t) = \omega_o + \delta\omega_m \cos(\omega_m t + 2\pi/3), \omega_3(t) = \omega_o + \delta\omega_m \cos(\omega_m t + 4\pi/3)$.

The internal power loss for a perfect circulator (infinite isolation and no reflection) constructed with three coupled cavities can be calculated from the external and ohmic Q (Qe and Qo, respectively) of the individual resonators. For a single resonator the fractional power loss is given by Ql/Qo where 1/Ql = 1/Qo + 1/Qe. Since the same power flows through two cavities (the third cavity power is zero since it is the isolated port) the total loss is 2 Ql/Qo and it would appear desirable to design for Qe<<Qo to minimize the insertion loss. However, computations show that as Qe is increased, reflection from the input port decreases and isolation increases for the optimal values of ω_m and $\delta\omega_m$ resulting in a decrease in insertion loss because of the decrease in reflection and increase in isolation. In addition, for Qe<<Qo, the fractional power loss is given by ~2 Qe/Qo, so the ohmic losses increase with increasing Qe resulting in an overall higher insertion loss, with the optimum occurring with Qe/Qo ≈0.033, resulting in an ohmic loss of 6.5%.

Increases in coupling factor *k* results in better circulator performance (higher isolation factor) at the optimal values of ω_m and $\delta\omega_m$. The optimal value of $\delta\omega_m$ increases with *k* so if the available modulation depth of a particular design is not sufficient to reach optimal value then further increases in *k* do not enhance the circulator performance. A typical calculation for circulator parameters of interest (reflection, insertion loss and isolation) versus modulation rate and depth is shown in Figure 6.

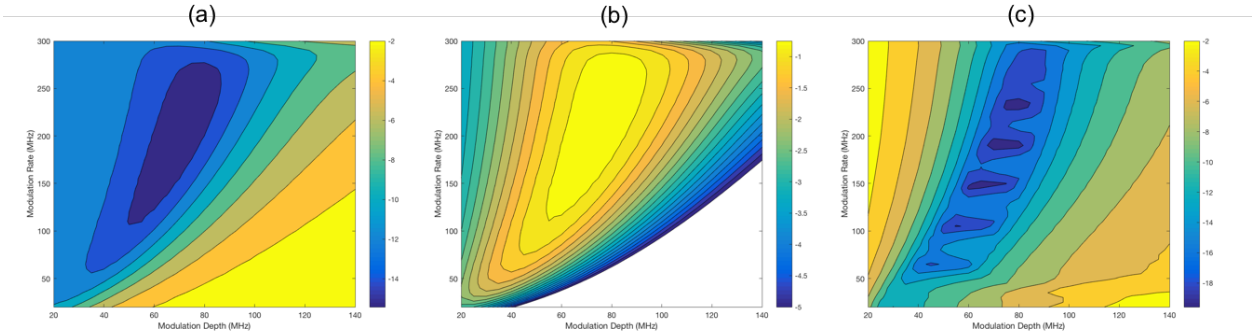

Figure 6 Response of modulated three port structure versus modulation depth and amplitude. Qe = 100, Qo = 6000 and k = 200. (a) Return loss (dB) (b) Insertion loss (dB) (c) Isolation (dB).

Design

The objective of our program is design of a high-power S band circulator. We started the design by evaluation of what values of coupling factor *k* can be obtained for different configurations of three coupled rectangular cavities in S-band relevant waveguide structures (Figure 7). The radial ring of cavities coupled by a cylindrical guide (Figure 7c) in the center had the maximum coupling value.

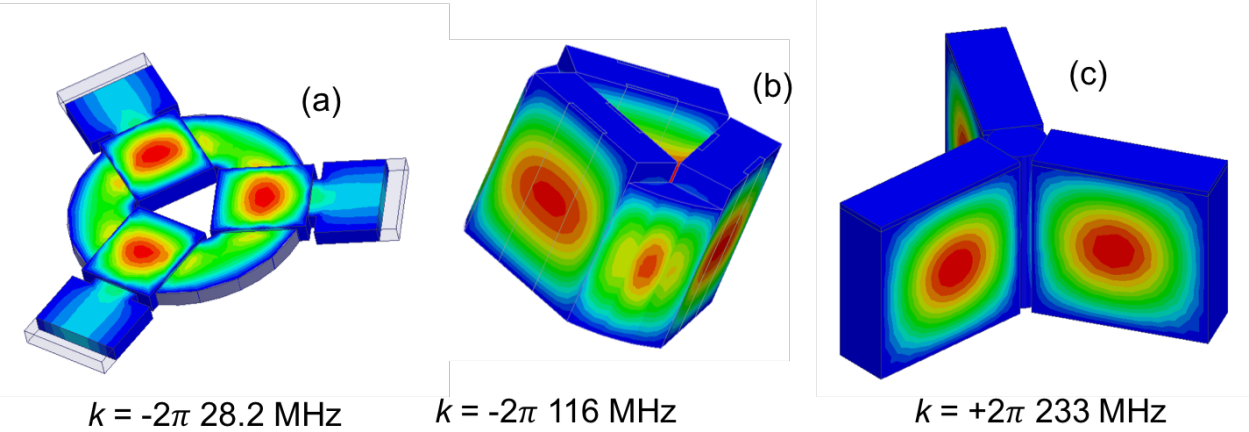

Figure 7 Three different coupling geometries based on rectangular cavities examined to find configuration with maximum coupling factor k.

An alternative configuration using coupled coaxial cavities was also examined but found to have spurious resonances inside the coupling bandwidth of the primary mode. The presence of the spurious mode would result in power loss from coupling of working mode to the spurious mode, so the coaxial configuration approach was abandoned.

Using the cavity configuration of Figure 7c with a thin slab of dielectric material on the upper wall of the three cavities (Figure 8) to provide modulation of the cavity frequency, we then determined the magnitude of frequency shift that could be induced in the cavity by changing the dielectric constant. The absolute value of the dielectric constant (120) and range of variation (120 to 150, 25% range) was chosen to match what is possible using a high-power ferroelectric material whose dielectric constant can be varied by applied electric field. This material and method proposed to vary dielectric constant are discussed in the appendix. A large number of variations of this configuration were evaluated for achievable modulation depth and coupling factor versus changes in the width, height and depth of the rectangular cavities, with a goal to maximize *k* and modulation depth. In all examined variations, it was found that as the achievable modulation depth was increased (by increasing thickness of dielectric material) the coupling factor *k* was reduced. A representative result of this sweep of dielectric slab thickness is shown in Table 1.

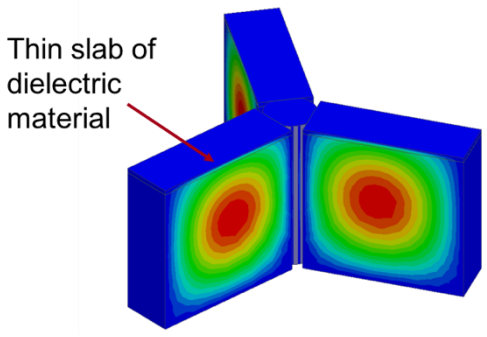

Figure 8 Three coupled cavities loaded with dielectric material.

Table 1 Calculated values of Q, k and modulation depth $\delta\omega_m$ for slab loaded, coupled cavity structure. The rectangular sections have dimensions of 60 mm W X 58 mm H X 20 mm D . The cavity ohmic Q and coupling factor k vary with value of dielectric constant, average of max and min values shown. The value in the last column is the frequency separation of lowest higher order cavity mode from the rotating mode. This separation should be much less than modulation depth and rate to avoid coupling power into the spurious mode.

Slab thickness (mm)	Average Qo	Average k (2π MHz)	Modulation Depth $\delta\omega_m$ (2π MHz)	Frequency Separation of Lowest Spurious Mode (MHz)
1.75	9150	+190	10	725
2.00	4950	+127	25	685
2.25	2640	+83	50	403

For the three cases of Table 1, the peak isolation value was determined within the range of the calculated peak modulation depth. The isolator parameters of interest for these cases are shown in Table 2.

Table 2 Calculated circulator parameters versus slab thickness. Qe set to .033 Qo for minimum insertion loss.

Slab thickness (mm)	Modulation Depth $\delta\omega_m$ (2π MHz)	Return Loss (dB)	Insertion Loss (dB)	Ohmic Loss %	Isolation (dB)
1.75	10	-9.8	-2.3	6.7	-12.5
2.00	25	-12.5	-1.3	6.8	-15.4
2.25	45	-10.9	-1.6	6.6	-15.0

An alternative configuration (Figure 9) using photonic bandgap (PBG) type structures was also examined. This approach was evaluated, as the PBG structure can be designed to move spurious mode resonances significantly beyond the bandwidth of the modulation rate. This was achieved with frequency separation from the lowest spurious mode of over 1 GHz. In addition, high modulation depth (2π 80 MHz) was also obtained at a high k factor (2π 220 MHz). Unfortunately, Qo for this case was low (1450), and the resulting performance (return loss -12.9 dB, insertion loss -1.3 dB and isolation -14.3 dB) did not exceed the best case obtained with the rectangular cavities.

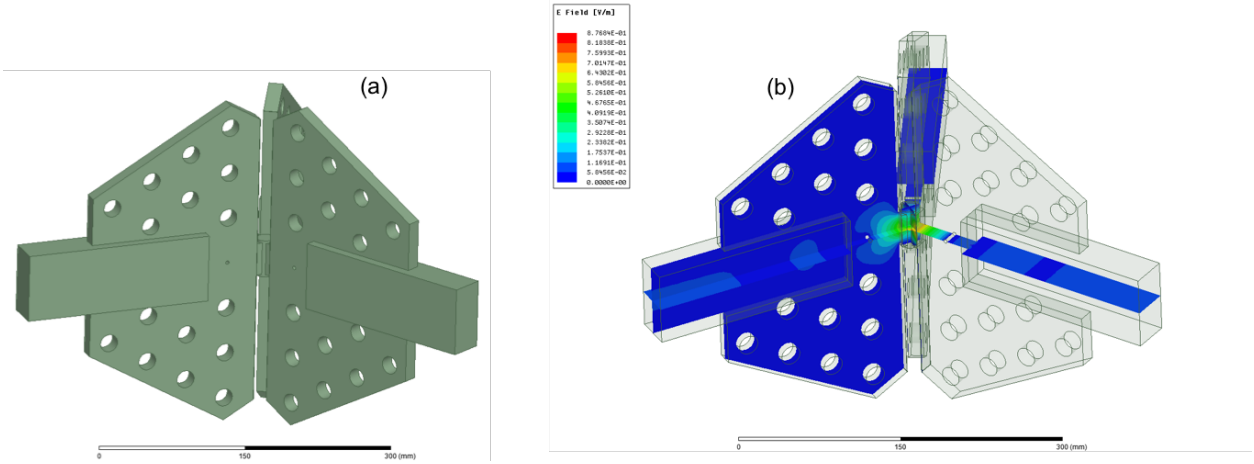

Figure 9 PBG cavity embodiment of circulator. (a) External surface showing rectangular waveguide coupling to cavities. The three cavities are coupled together by small cylindrical section at center and a dielectric layer was placed on the long wall facing the inner cylindrical section. (b) Electric field in PBG structure.

Conclusion

Multiple configurations for a waveguide based implementation of the ferrite free circulator concept were evaluated. The best performance obtained (return loss -12.5 dB, insertion loss -1.3 dB and isolation -15.4 dB) is not good enough to warrant further investigation of this approach unless new techniques and lower loss material can be found that could increase k and $\delta\omega_m$ to levels that result in adequate performance. For high power klystron applications, a typical acceptable performance level would be return and isolation < -20 dB and an insertion loss < 0.5 dB. Obtaining this level of performance for the second case of Table 1 (2mm slab thickness) would have required $k > 2\pi$ 250 MHz and $\delta\omega_m > 2\pi$ 50 MHz. At this point it is not clear to the authors how to obtain those values with existing materials using the evaluated circuit configurations.

Appendix: Ferroelectric Loading of Cavity for Resonant Frequency Modulation

One option for varying the resonant frequency of a waveguide based cavity is loading the cavity with a ferroelectric material. Response times for these materials is approximately 10^{-11} sec for crystalline material and approximately 10^{-10} sec for ceramic compounds [3,4]. This would support modulation rates into the GHz frequency range. These materials also exhibit high dielectric breakdown strength and low gas permeability. Several high-power waveguide devices using these ferroelectric materials for dynamic tuning of phase shifting and resonant frequency tuning were constructed and tested [5,6]. Figure 10 shows a possible configuration that could be used in the proposed circulator.

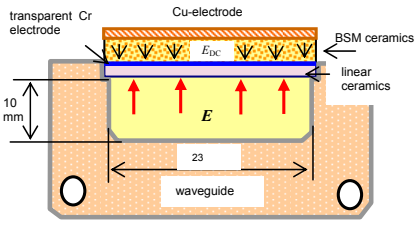

Figure 10 Ferroelectric loaded waveguide. The bias field is applied between the waveguide and Cu-electrode on top of the BSM ceramic (ferroelectric material).

References

1. Estep, Nicholas A., et al. "Magnetic-free non-reciprocity and isolation based on parametrically modulated coupled-resonator loops." *Nature Physics* 10.12 (2014): 923-927.
2. Wonjoo Suh, Zheng Wang and Shanhui Fan ,"Temporal Coupled-Mode Theory and the Presence of Non-Orthogonal Modes in Lossless Multimode Cavities, IEEE Journal of Quantum Elec, Vol 40, No. 10, Oct 2004
3. G.A. Smolensky, Ferroelectrics and Related Materials, Academic Press, New York, (1981).
4. A.K. Tagantsev et al. Journal of Electroceramics 11, pp. 5-66, 2003
5. Kanareykin, A., et al. "Ferroelectric Based High Power Tuner for L-Band Accelerator Applications." (2013).
6. Kanareykin, A., et al. "Experimental Demonstration of an X-Band Tunable Dielectric Accelerating Structure." Particle Accelerator Conference, 2005. PAC 2005. Proceedings of the. IEEE, 2005.